Operation Strategy of Rail Transit Green Energy System Considering Uncertainty Risk of Photovoltaic Power Output

Yanbo Chen, *Senior Member*, *IEEE*, Haoxin Tian, *Student Member*, *IEEE*, Guodong Zheng, Yuxiang Liu, and Maja Grbić

Abstract—The integration of photovoltaic power generation is a new development into the traction power supply system (TPSS). However, traditional research on the TPSS operation strategy has not fully considered the risk of uncertainty in photovoltaic power output. To this end, we propose an operation strategy for the rail transit green energy system that considers the uncertainty risk of photovoltaic power output. First, we establish a regenerative braking energy utilization model that considers the impact of time-of-use (TOU) electricity price on the utilization efficiency and economic profit of regenerative braking energy and compensates for non-traction load. Then, we propose an operation strategy based on the balance of power supply and demand that uses an improved light robust (ILR) model to minimize the total cost of the rail transit green energy system, considering the risk of uncertainty in photovoltaic power output. The model incorporates the two-step load check on the second-level time scale to correct the operational results, solve the issue of different time resolutions between photovoltaic power and traction load, and achieve the coordinated optimization of risk cost and operation cost after photovoltaic integration. Case studies demonstrate that the proposed model can effectively consider the impact of the uncertainty in photovoltaic power output on the operation strategy, significantly improving the efficiency and economy of the system operation.

***Index Terms*—Rail transit green energy system, improved light robust (ILR) optimization, two-step load check, time resolution, operation strategy.**

I. Introduction

In China, the railway industry has high and increasing carbon footprint year by year, and there is a huge potential for carbon reduction throughout the life cycle [1]. The academic community has recently proposed integrating photovoltaic power generation into the traction power supply system (TPSS) to promote carbon reduction in the railway industry. This initiative has multiple benefits: it fully utilizes the natural resources around the railway, promotes the energy self-sufficient of the TPSS, ensures the normal operation of rail transit during power grid outages, and reduces the carbon footprint to assist in achieving the carbon peaking and carbon neutrality goals [2]-[4]. However, the inevitable prediction error of photovoltaic power output results in uncertainty on the supply side of the TPSS, which increases the operational risk of the system. Developing the operation strategy of the rail transit green energy system that considers both operational risk and cost is an urgent issue to be addressed.

As photovoltaic power generation technology is still a cutting-edge field of research, most studies have primarily focused on distributed photovoltaic power generation systems, photovoltaic power stations, and microgrids, among others. There is a notable dearth of research exploring the TPSS with photovoltaic integration [5]. In the non-traction field, existing studies primarily investigate the utilization of photovoltaic power generation to power communication and signal systems at stations [6], [7]. In the traction field, current research on the TPSS with photovoltaic integration mainly focuses on overall system design and control strategy under different operational conditions [8]. Reference [9] proposes a relatively simple photovoltaic integration scheme using single-phase inverters connected to the traction feed line. Reference [10] proposes a three-phase photovoltaic integration topology and its control method, which effectively integrates the photovoltaic power system based on the basic principles of the TPSS. Reference [11] proposes a control method for a complex electrified railway system with photovoltaic integration from the perspective of the topology of the TPSS, focusing on the Sichuan-Tibet Railway. Reference [12] analyzes the impact of photovoltaic integration on the TPSS from multiple aspects, including the adaptability of photovoltaic

Manuscript received: October 24, 2023; revised: January 11, 2024; accepted: March 17, 2024. Date of CrossCheck: March 17, 2024. Date of online publication: April 9, 2024.

This work was supported in part by the National Key Research and Development Program of China (No. 2021YFB2601502) and in part by the Beijing Natural Science Foundation Program (No. L221002).

Y. Chen (corresponding author), H. Tian, G. Zheng, and Y. Liu are with the State Key Laboratory of Alternate Electrical Power System with Renewable Energy Sources, North China Electric Power University, Beijing 102206, China, and Y. Chen is also with the School of Engineering, Qinghai University of Technology, Xining 810016, China, and the New Energy (Photovoltaic) Industry Research Center and the Key Laboratory for Smart Operation of New Energy Power System of the Ministry of Education, Qinghai University, Xining 810016, China (e-mail: chenyanbo@ncepu.edu.cn; haoxin_tian@ncepu.edu.cn; 826107954@qq.com; lyxbgyx@163.com).

M. Grbić is with the Nikola Tesla Electrical Engineering Institute, University of Belgrade, Belgrade 11000, Serbia (e-mail: maja.grbic@ieent.org).

DOI: 10.35833/MPCE.2023.000788

inverters, the interaction influence of harmonic-negative sequence current and reactive power, the voltage stability of the traction network, the consumption of photovoltaic energy, and the feedback of regenerative braking energy, among other energy management problems. Unlike general power loads, the traction load also includes a portion of regenerative braking energy, which is an important part of the operation strategy. Reference [13] proposes two regenerative braking energy utilization schemes of energy storage type and energy feedback type based on the characteristics of traction load. Reference [14] proposes a bypass DC circuit-based idea for utilizing regenerative braking energy in urban rail transit. However, these studies do not adequately consider the risk associated with the uncertainty of photovoltaic power output. In addition, there is a lack of detailed models for the optimal coordination of the photovoltaic power system, energy storage, and power grid in the TPSS.

Research on the uncertainty of photovoltaic power output and the resulting operational risk has mainly focused on power dispatch, using methods such as stochastic optimization and robust optimization (RO). Stochastic optimization requires generating typical scenarios based on the probability of uncertain parameters [15], [16]. This often requires a significant amount of historical data and may not suit incomplete or newly constructed photovoltaic power stations. In contrast, RO does not require knowledge of the probability distribution function of uncertain parameters and describes the fluctuation range of parameters through an uncertain set. This makes it more widely applicable but also more conservative. Many studies have improved the conservatism of the traditional RO model. For example, [17] proposes a robust model that considers the operational risk and demand response, which improves the conservatism of the model by dynamically adjusting the output boundaries of wind power. Reference [18] focuses on the constraint violation and adjusts the conservatism of the solution by limiting the deviation of the objective function. Based on [18], [19] proposes an improved light robust (ILR) model that allows for certain constraint violations to improve solution conservatism and prevent excessive violation. The proposed model has been applied in [20] and [21].

On the load side of the TPSS, the traction load shows strong fluctuations and shock characteristics that change suddenly in response to changes under train operation conditions [22]. To address this issue, [23] proposes a traction load prediction method that treats dynamic traction load as an ordered combination of the time slots provided by the train running timetable. Reference [24] presents a traction load prediction method based on analyzing the main characteristic parameters of traction load from measured data. The aforementioned studies indicate that although traction load is strongly fluctuating and random, it can be roughly determined by the train running timetable and historical data within a specific period and operation interval, showing a certain level of predictability. In contrast, although current photovoltaic power prediction can achieve high accuracy, the prediction error of photovoltaic power output is unavoidable and significant, as it is heavily dependent on changes in the natural environment [25].

This paper studies the operation strategy of the rail transit green energy system considering the uncertainty risk of photovoltaic power output. It introduces a regenerative braking energy utilization model, which considers the impact of time-of-use (TOU) electricity price on the utilization efficiency and economic profit of regenerative braking energy and can compensate for non-traction load. This paper also constructs an ILR model to minimize the total cost and balance the power supply and demand of the rail transit green energy system.

This paper makes three main contributions.

1) We propose an ILR model for the rail transit green energy system considering the uncertainty of photovoltaic power output. This model optimizes risk cost and operation cost in coordination, offering a solution for the low-carbon rail transit green energy system.

2) We propose a regenerative braking energy utilization model that considers the impact of TOU electricity price on the efficiency and economy of regenerative braking energy.

3) We establish a power supply and demand balance model that accounts for the risk of photovoltaic operation and the fluctuation of traction load. This model incorporates the two-step load check on the second-level time scale to correct the operational results and solve the issue of different time resolutions between photovoltaic power and traction load.

The rest of this paper is organized as follows. Section II introduces the structure of the rail transit green energy system. Section III models the operation strategy of the rail transit green energy system. The model solving strategy is presented in Section IV. Case studies are shown in Section V, and conclusions are drawn in Section VI.

II. Structure of Rail Transit Green Energy System

This section presents a typical structure of the rail transit green energy system, as shown in Fig. 1.

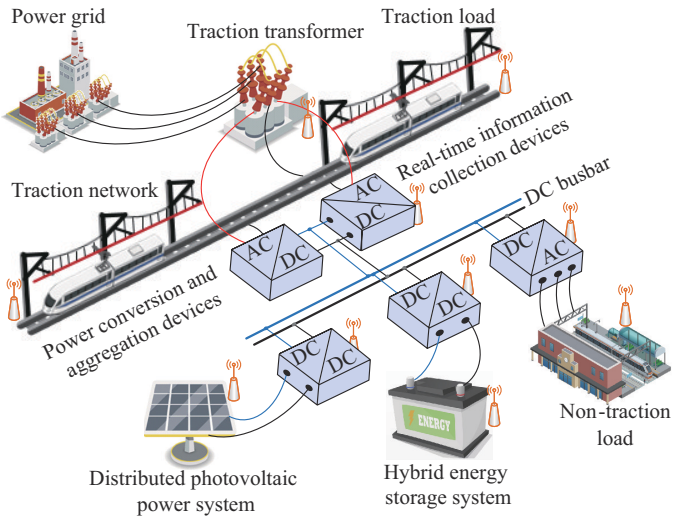

Fig. 1. Structure of rail transit green energy system.

The distributed photovoltaic power system is installed in the traction substation and on both sides of the railway to op-

timize the energy utilization of rail transit assets. The hybrid energy storage system is configured as needed to effectively utilize regenerative braking energy and meet the balance of power supply and demand. As an intermediate link, power electronic devices can achieve power conversion and aggregation. The traction transformer introduces clean electricity into the traction network, enabling the gradual transformation of the traditional TPSS to the rail transit green energy system. The system uses real-time information collection devices to achieve the "network−source−storage−vehicle" collaborative energy supply for rail transit [26].

A. Characteristics of Traction Load

Compared with general power loads, the traction load has strong fluctuations. Through analysis of the measured traction load of a traction substation, as shown in Fig. 2, it can be observed that the load is relatively large with a maximum instantaneous power of 51.27 MW. The power changes frequently with peaks and valleys, and the energy consumption is high with a daily consumption of 392.9 MWh. When the traction load is less than 0, it indicates that the train is under the braking condition, and regenerative energy is fed back to the traction network. In addition, traction load is closely related to the train running timetable, and thus accurate prediction can be achieved.

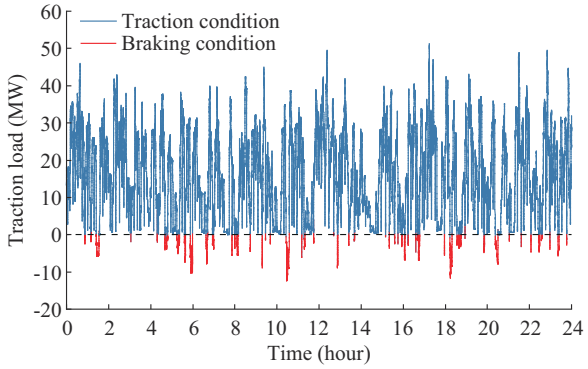

Fig. 2. Measured traction load.

B. ILR Model Considering Risk Cost of Photovoltaic Power Output

In this subsection, a budgeted uncertain set of photovoltaic power output is constructed and an ILR model that considers the risk cost of photovoltaic power output is established.

1) ILR Model

According to the distribution characteristics of the photovoltaic power system along the railway, the output of a photovoltaic power system can be decomposed into the sum of the output of multiple photovoltaic units. The photovoltaic power output constraint can be expressed as:

$$P_T^{\mathrm{PV}} \le \sum_{j=1}^{k} P_{jT}^{\mathrm{PV}} \tag{1}$$

where P_T^{PV} is the output of the photovoltaic power system during period T; P_{jT}^{PV} is the output of photovoltaic unit j during period T; and k is the total number of photovoltaic units.

Considering the uncertainty of photovoltaic power output, the output of photovoltaic units can be expressed as the expected value plus fluctuation term, while setting the total fluctuation amount during different periods as:

$$\begin{cases} P_T^{\mathrm{PV}} - \gamma_T \le \sum_{j=1}^{k} \left(\bar{P}_{jT}^{\mathrm{PV}} + \zeta_{jT} \tilde{P}_{jT}^{\mathrm{PV}} \right) \\ \left| \zeta_{jT} \right| \le 1 \\ \sum_{j=1}^{k} \left| \zeta_{jT} \right| \le \Gamma_T \end{cases} \tag{2}$$

where γ_T is the slack variable during period T, representing the degree of the constraint violation; $\bar{P}_{jT}^{\mathrm{PV}}$ is the expected output of photovoltaic unit j during period T; $\tilde{P}_{jT}^{\mathrm{PV}}$ is the maximum amplitude of fluctuation in the output of photovoltaic unit j during period T; ζ_{jT} is the proportion of fluctuation in the output of photovoltaic unit j during period T; and Γ_T is the total fluctuation amount during period T.

Then, we transform the photovoltaic power output constraint into its tractable linear counterpart with a budgeted uncertain set using the sorting truncation method in [12], which is expressed as:

$$\begin{cases} P_T^{\mathrm{PV}} - \gamma_T \le \sum_{j=1}^{k} \bar{P}_{jT}^{\mathrm{PV}} - \sum_{j=1}^{\lfloor \Gamma_T \rfloor} \left| \tilde{P}_{jT}^{\mathrm{PV}'} \right| - \left(\Gamma_T - \lfloor \Gamma_T \rfloor \right) \left| \tilde{P}_{\lfloor \Gamma_T \rfloor + 1, T}^{\mathrm{PV}'} \right| \\ \Delta P_T = \sum_{j=1}^{\lfloor \Gamma_T \rfloor} \left| \tilde{P}_{jT}^{\mathrm{PV}'} \right| + \left(\Gamma_T - \lfloor \Gamma_T \rfloor \right) \left| \tilde{P}_{\lfloor \Gamma_T \rfloor + 1, T}^{\mathrm{PV}'} \right| \\ 0 \le \gamma_T \le 2\Delta P_T \end{cases} \tag{3}$$

where $\lfloor \Gamma_T \rfloor$ is the greatest integer that is less than or equal to Γ_T; $[-\Delta P_T, \Delta P_T]$ is the fluctuation range of the overall output of the photovoltaic power system during period T; and $\left| \tilde{P}_{jT}^{\mathrm{PV}'} \right|$ is an element in the sequence $\left\{ \left| \tilde{P}_{1T}^{\mathrm{PV}} \right|, \left| \tilde{P}_{2T}^{\mathrm{PV}} \right|, ..., \left| \tilde{P}_{kT}^{\mathrm{PV}} \right| \right\}$ after descending order.

Compared with the traditional RO model, the ILR model described above can reflect the predictive accuracy of the photovoltaic power output by controlling the total fluctuation amount, and its tractable linear counterpart with a budgeted uncertain set can improve the applicability of the model. Additionally, the ILR model extends the traditional RO problem that solely focuses on operation cost to an optimization problem that considers both risk cost and operation cost. The objective function is as follows:

$$\min_{\boldsymbol{x}, \boldsymbol{\gamma}} \left(\boldsymbol{c}^{\mathrm{T}} \boldsymbol{x} + \boldsymbol{\omega}^{\mathrm{T}} \boldsymbol{\gamma} \right) \tag{4}$$

where $\boldsymbol{c}^{\mathrm{T}} \boldsymbol{x}$ is the original objective function of the optimization problem, representing operation cost; $\boldsymbol{\omega}^{\mathrm{T}} \boldsymbol{\gamma}$ is the cost of constraint violation, representing risk cost of the photovoltaic power output; and $\boldsymbol{\omega}$ is the weight coefficient vector of the slack variable, a higher value of which implies a greater cost for constraint violation.

2) Risk Cost Analysis of Slack Variable

Generally, the larger the slack variable, the higher the risk cost, resulting in the increasing weight coefficient as the slack variable increases. Considering that it is difficult to obtain the true probability distribution of the photovolta-

ic power output, we divide the confidence interval of the photovoltaic power output into the low-risk area and the high-risk area based on the expected power output, as shown in Fig. 3.

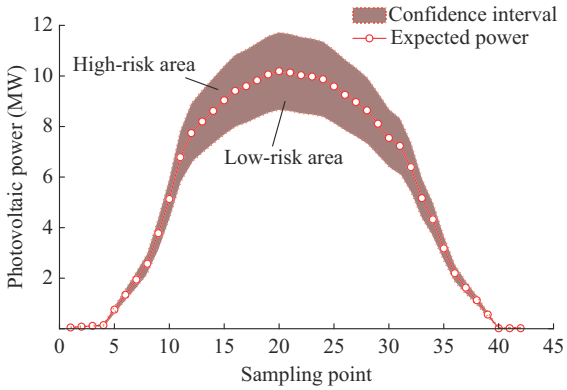

Fig. 3. Risk distribution of slack variable.

When the photovoltaic power output is in the low-risk area, a smaller weight coefficient is assigned, while a larger weight coefficient is assigned when in the high-risk area. And the risk cost during period T is calculated as:

$$\omega_T\gamma_T=\begin{cases}\omega_T^{\mathrm{L}}\gamma_T & 0\le\gamma_T\le\Delta P_T\\ \omega_T^{\mathrm{L}}\Delta P_T+\omega_T^{\mathrm{H}}\left(\gamma_T-\Delta P_T\right) & \Delta P_T<\gamma_T\le 2\Delta P_T\end{cases}\tag{5}$$

where ω_T is the weight coefficient during period T; and ω_T^{L} and ω_T^{H} are the weight coefficients in the low-risk area and the high-risk area during period T, respectively.

In this paper, we define the value of the weight coefficient as obtained by multiplying the electricity price by the risk scaling factor, which can be expressed as:

$$\begin{cases}\omega_T^{\mathrm{L}}=b_1G_T\\ \omega_T^{\mathrm{H}}=b_2G_T\end{cases}\tag{6}$$

where G_T is the electricity price during period T; and b_1 and b_2 are the risk scaling factors of the photovoltaic power output in the low-risk area and the high-risk area, respectively. When the risk scaling factor is less than 1, it indicates that the risk of photovoltaic power output is small, and the absorption of photovoltaic power is encouraged.

III. Operation Strategy of Rail Transit Green Energy System

A. Conversion of Time Resolution

According to [27], the time resolution requirement for photovoltaic power prediction data is 15 min, while the time resolution of the measured data of traction load is mostly 1 s, indicating a mismatch in time resolution. The conversion of power data in terms of time resolution is formulated as:

$$\begin{cases}\Delta T\to\Delta t{:}P_t^{\mathrm{x}}=P_T^{\mathrm{x}} & t\in\left[n(T-1)+1,nT\right]\\ \Delta t\to\Delta T{:}P_T^{\mathrm{x}}=\dfrac{\sum_{t=T}^{T+n\Delta t-1}P_t^{\mathrm{x}}}{n} & n=\dfrac{\Delta T}{\Delta t}\end{cases}\tag{7}$$

where Δt and ΔT are the time resolutions of 1 s and 15 min, respectively; P_t^{x} and P_T^{x} are the power data with time resolutions of Δt and ΔT, respectively; and the superscript x can represent any element.

B. Regenerative Braking Energy Utilization Model

1) Objective Function

The train under the braking condition generates a large amount of regenerative energy, which can be collected by supercapacitor energy storage (SCES). Considering the impact of the TOU electricity price on the utilization efficiency and economic profit of regenerative braking energy, the objective function under the braking condition is set to maximize the utilization of regenerative braking energy through SCES under the guidance of the TOU electricity price, as shown in (8).

$$\max G_T^{\mathrm{TOU}}\left|P_T^{\mathrm{SCES}}\right|\Delta T\tag{8}$$

where G_T^{TOU} is the TOU electricity price during period T; and P_T^{SCES} is the power of SCES during period T, which is negative in charging status and positive in discharging status.

2) Prevailing Constraints

The prevailing constraints under the braking condition include the state of charge (SOC) limits of SCES (9) and (10), the equal capacity limit of SCES at the beginning and end of each day (11), and the charging and discharging power limit of SCES (12).

$$S_{\mathrm{L}}^{\mathrm{SCES}}E_{\mathrm{M}}^{\mathrm{SCES}}\le E_T^{\mathrm{SCES}}\le S_{\mathrm{H}}^{\mathrm{SCES}}E_{\mathrm{M}}^{\mathrm{SCES}}\tag{9}$$

$$E_T^{\mathrm{SCES}}=E_0^{\mathrm{SCES}}-\sum_{T'=1}^{T}P_{T'}^{\mathrm{SCES}}\Delta T\tag{10}$$

$$E_{96}^{\mathrm{SCES}}=E_0^{\mathrm{SCES}}\tag{11}$$

$$P_T^{\mathrm{RB}}\le P_T^{\mathrm{SCES}}\le P_{\mathrm{M}}^{\mathrm{SCES}}\tag{12}$$

where $S_{\mathrm{L}}^{\mathrm{SCES}}$ and $S_{\mathrm{H}}^{\mathrm{SCES}}$ are the minimum and maximum SOCs of SCES, respectively; E_0^{SCES} and E_{96}^{SCES} are the initial and final capacities of SCES, respectively; E_T^{SCES} is the capacity of SCES during period T; $E_{\mathrm{M}}^{\mathrm{SCES}}$ and $P_{\mathrm{M}}^{\mathrm{SCES}}$ are the rated capacity and power of SCES, respectively; and P_T^{RB} is the limited charging power of SCES under the braking condition during period T.

Considering that the charging power of SCES should not exceed the regenerative braking energy during the corresponding period, P_T^{RB} is calculated as:

$$P_T^{\mathrm{RB}}=\frac{\sum_{t=T}^{T+n\Delta t-1}P_t^{\mathrm{RB}}}{n}\tag{13}$$

$$P_t^{\mathrm{RB}}=\begin{cases}P_t^{\mathrm{RB0}} & P_t^{\mathrm{RB0}}>-P_{\mathrm{M}}^{\mathrm{SCES}}\\ -P_{\mathrm{M}}^{\mathrm{SCES}} & P_t^{\mathrm{RB0}}\le-P_{\mathrm{M}}^{\mathrm{SCES}}\end{cases}\tag{14}$$

where P_t^{RB0} is the regenerative braking power during period t, which is negative in the traction load.

3) Compensation for Non-traction Load

Aside from the traction load, non-traction loads such as air conditioning, lighting, electric heating, communication, and signal systems coexist within the traction substation. Utilizing regenerative braking energy can compensate for non-traction load, then we have:

$$D_T^{\mathrm{f}}=\begin{cases}D_T^{\mathrm{ff0}} & P_T^{\mathrm{SCES}}<0\\ D_T^{\mathrm{ff0}}-P_T^{\mathrm{SCES}} & P_T^{\mathrm{SCES}}\geq 0\end{cases} \tag{15}$$

where D_T^{ff0} and D_T^{f} are the non-traction loads during period T before and after compensation, respectively.

Meanwhile, the utilization efficiency of regenerative braking energy is defined as:

$$\eta=\frac{\sum_{T=1}^{96}\left(D_T^{\mathrm{ff0}}-D_T^{\mathrm{f}}\right)\Delta T}{\sum_{t=1}^{86400}\left|P_t^{\mathrm{RB0}}\right|\Delta t}\times 100\% \tag{16}$$

where $\sum_{T=1}^{96}\left(D_T^{\mathrm{ff0}}-D_T^{\mathrm{f}}\right)\Delta T$ represents the regenerative braking energy utilized by SCES; and $\sum_{t=1}^{86400}\left|P_t^{\mathrm{RB0}}\right|\Delta t$ represents the total regenerative braking energy in the traction load.

Then, the economic profit generated by SCES utilizing regenerative braking energy is given by:

$$C_0=\sum_{T=1}^{96}\left[G_T^{\mathrm{TOU}}\left(D_T^{\mathrm{ff0}}-D_T^{\mathrm{f}}\right)-W_{\mathrm{C}}^{\mathrm{SCES}}\left|P_T^{\mathrm{SCES}}\right|\right]\Delta T \tag{17}$$

where $W_{\mathrm{C}}^{\mathrm{SCES}}$ is the cost per MWh of electricity generated by SCES.

C. Power Supply and Demand Balance Model Based on ILR Optimization

1) Objective Function

Considering the uncertainty of photovoltaic power output and the resulting operational risk, lithium-ion battery energy storage (LBES) is needed to meet the balance of power supply and demand under the traction condition. Instead of the TOU electricity price, the two-part electricity price is adopted for traction load. The objective function under the traction condition is set to minimize the total cost of the rail transit green energy system, as shown in (18).

$$\min C_{\mathrm{total}}=C_{\mathrm{operation}}+C_{\mathrm{risk}} \tag{18}$$

$$\begin{cases}C_{\mathrm{operation}}=C_1+C_2-C_3-C_0\\ C_1=\sum_{T=1}^{96}G_T P_T^{\mathrm{G}}\Delta T\\ C_2=\sum_{T=1}^{96}\left(W_{\mathrm{C}}^{\mathrm{LBES}}\left|P_T^{\mathrm{LBES}}\right|-W_{\mathrm{D},T}^{\mathrm{LBES}}P_T^{\mathrm{LBES}}\right)\Delta T\\ W_{\mathrm{D},T}^{\mathrm{LBES}}=\frac{D_T^{\mathrm{q}}-\bar{D}^{\mathrm{q}}}{\bar{D}^{\mathrm{q}}}W_{\mathrm{D}}^{\mathrm{LBES}}\\ \bar{D}^{\mathrm{q}}=\frac{\sum_{T=1}^{96}D_T^{\mathrm{q}}}{96}\\ C_3=\sum_{T=1}^{96}W_{\mathrm{V}}^{\mathrm{PV}}P_T^{\mathrm{PV}}\Delta T\\ C_{\mathrm{risk}}=\sum_{T=1}^{96}\omega_T\gamma_T\Delta T\end{cases} \tag{19}$$

where $C_{\mathrm{operation}}$ is the operation cost; C_{risk} is the risk cost; C_1 is the cost of purchasing electricity from the power grid; C_2 is the cost of LBES; C_3 is the subsidy for distributed photovoltaic power generation; P_T^{G} is the power output of the power grid during period T; P_T^{LBES} is the power of LBES during period T; D_T^{q} is the traction load during period T; $\bar{D}^{\mathrm{q}}$ is the average traction load within a day; $W_{\mathrm{C}}^{\mathrm{LBES}}$ is the cost per MWh of electricity generated by LBES; $W_{\mathrm{D}}^{\mathrm{LBES}}$ is the profit per MWh of electricity generated by LBES; $W_{\mathrm{D},T}^{\mathrm{LBES}}$ is the adjusted value for $W_{\mathrm{D}}^{\mathrm{LBES}}$ during period T; and $W_{\mathrm{V}}^{\mathrm{PV}}$ is the subsidy per MWh of electricity generated by distributed photovoltaic power system.

In this paper, P_T^{LBES} is negative in charging status and positive in discharging status. When the traction load is at its peak, $W_{\mathrm{D},T}^{\mathrm{LBES}}$ is positive, and LBES should be in discharging status to generate profit; when the traction load is at its valley, $W_{\mathrm{D},T}^{\mathrm{LBES}}$ is negative, and LBES should be in charging status to generate profit. Therefore, the setting of $W_{\mathrm{D},T}^{\mathrm{LBES}}$ helps guide LBES for peak shaving and valley filling.

2) Prevailing Constraints

In addition to photovoltaic power output constraint (3), the prevailing constraints under the traction condition also include the power balance limit of the system (20), the power limit of the traction transformer (21), the SOC limit of LBES (22) and (23), the equal capacity limit of LBES at the beginning and end of each day (24), and the charging and discharging power limit of LBES (25).

$$P_T^{\mathrm{G}}+P_T^{\mathrm{LBES}}+P_T^{\mathrm{PV}}=D_T^{\mathrm{q}}+D_T^{\mathrm{f}} \tag{20}$$

$$0\leq P_T^{\mathrm{G}}\leq P_{\mathrm{M}}^{\mathrm{G}} \tag{21}$$

$$S_{\mathrm{L}}^{\mathrm{LBES}}E_{\mathrm{M}}^{\mathrm{LBES}}\leq E_T^{\mathrm{LBES}}\leq S_{\mathrm{H}}^{\mathrm{LBES}}E_{\mathrm{M}}^{\mathrm{LBES}} \tag{22}$$

$$E_T^{\mathrm{LBES}}=E_0^{\mathrm{LBES}}-\sum_{T'=1}^{T}P_{T'}^{\mathrm{LBES}}\Delta T \tag{23}$$

$$E_{96}^{\mathrm{LBES}}=E_0^{\mathrm{LBES}} \tag{24}$$

$$-P_{\mathrm{M}}^{\mathrm{LBES}}\leq P_T^{\mathrm{LBES}}\leq P_{\mathrm{M}}^{\mathrm{LBES}} \tag{25}$$

where $P_{\mathrm{M}}^{\mathrm{G}}$ is the rated power of the traction transformer; $S_{\mathrm{L}}^{\mathrm{LBES}}$ and $S_{\mathrm{H}}^{\mathrm{LBES}}$ are the minimum and maximum SOCs of LBES, respectively; E_0^{LBES} and E_{96}^{LBES} are the initial and final capacities of LBES, respectively; E_T^{LBES} is the capacity of LBES during period T; and $E_{\mathrm{M}}^{\mathrm{LBES}}$ and $P_{\mathrm{M}}^{\mathrm{LBES}}$ are the rated capacity and power of LBES, respectively.

IV. Model Solving Strategy

For the complex models mentioned above, this section presents a strategy to solve them. The flowchart is illustrated in Fig. 4, and it is described in detail in the following paragraphs.

A. Solution of Regenerative Braking Energy Utilization Model

Under the braking condition, the regenerative braking energy utilization model is a linear programming (LP) problem with a time resolution of 15 min, which can be efficiently solved by commercial optimization software. SCES is a power-type storage with fast response speed, which can easily meet the constraints with a time resolution of 1 s. Moreover, the compensated non-traction load in the solution results is used as the input for the power supply and demand balance model.

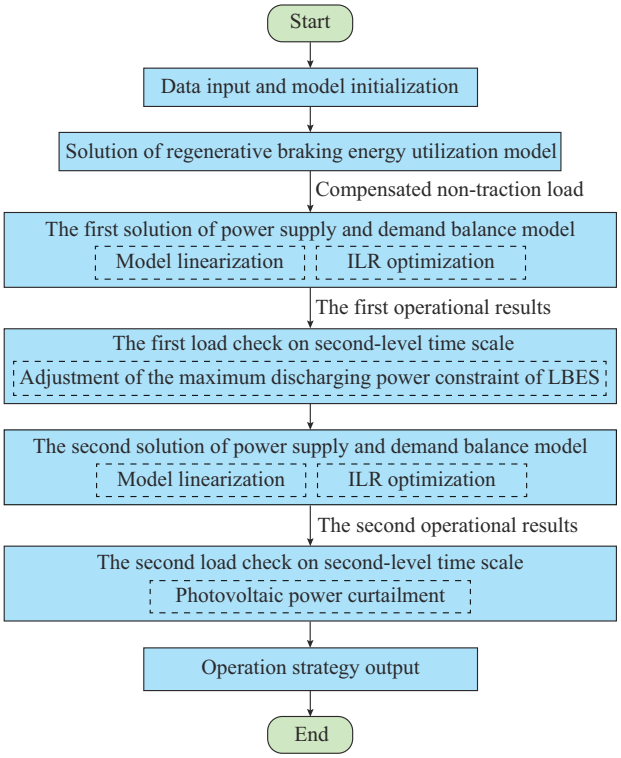

Fig. 4. Flowchart of model solving strategy.

B. Solution of Power Supply and Demand Balance Model Based on ILR Optimization

Under the traction condition, the risk cost in the objective function of the power supply and demand balance model with a time resolution of 15 min is nonlinear. As a result, the computational efficiency is not high and the global optimal solution cannot be conveniently obtained by commercial optimization software. In addition, LBES is an energy-type storage without fast response speed, which may violate the constraints with a time resolution of 1 s. To address the issue of different time resolutions between photovoltaic power and traction load, we propose a solving strategy that incorporates the two-step load check on the second-level time scale to correct the operational results.

1) Model Linearization

Assuming the photovoltaic power output is in the low-risk area, the model is converted to an LP problem owing to $0 \le \gamma_T \le \Delta P_T$, from which the solution of the slack variable γ'_T can be obtained. According to γ'_T, the risk cost of the photovoltaic power output can be adjusted as:

$$\omega_T \gamma_T = \begin{cases} \omega_T^{\mathrm{L}} \gamma_T & \gamma'_T < \Delta P_T \\ \omega_T^{\mathrm{L}} \Delta P_T + \omega_T^{\mathrm{H}} \gamma_T & \gamma'_T = \Delta P_T \end{cases} \tag{26}$$

$$0 \le \gamma_T \le \Delta P_T \tag{27}$$

Since γ'_T is known, the model is converted to an LP problem, and the operational results can be obtained with a time resolution of 15 min.

2) Two-step Load Check

Considering the scenario where the power grid is capable of meeting the demand independently, it is believed that the rated power of the traction transformer should be greater than the peak load. When the traction load with a time resolution of 1 s is above or slightly below its average value in 15 min, the power balance constraint of the system can be met by increasing or decreasing the output of the power grid, and constraint violation will not occur because the load variation is within a manageable range. When the traction load with a time resolution of 1 s is far lower than its average value in 15 min, it is insufficient to maintain the system power balance by only decreasing the output of the power grid, and constraint violation occurs at this time. To maximize the absorption of photovoltaic power, it is necessary to limit the discharging power of LBES. If it exceeds the regulation range of the power grid and LBES, the photovoltaic power curtailment has to be considered. To this end, a two-step load check method is proposed to correct the above operational results.

1) The first load check after the first model solution aims to adjust the maximum discharging power constraint for LBES.

Through (7), the photovoltaic power output and the compensated non-traction load in the first operational results with a time resolution of 15 min can be converted into the power with a time resolution of 1 s, and the discharging power of LBES with a time resolution of 1 s is generated according to its rated power. Then, the power output of the power grid with a time resolution of 1 s corresponding to the maximum discharging power of LBES is calculated as:

$$P_t^{\mathrm{G,I}} = D_t - P_t^{\mathrm{PV,I}} - P_{\mathrm{M}}^{\mathrm{LBES}} \tag{28}$$

where D_t is the comprehensive load during period t, which is obtained by adding traction load and compensated non-traction load with a time resolution of 1 s; and the superscript I represents the first load check process.

When $P_t^{\mathrm{G,I}} \ge 0$, it indicates that there is no constraint violation, the maximum discharging power constraint for LBES does not need to be adjusted during period t. When $P_t^{\mathrm{G,I}} < 0$, it indicates that there is a situation where the absorption of photovoltaic power is affected because the discharging power of LBES is too high, causing the constraint violation. Therefore, it is necessary to adjust the maximum discharging power of LBES during period t, as shown in (29).

$$P_{\mathrm{MD},t}^{\mathrm{LBES}} = \begin{cases} P_{\mathrm{M}}^{\mathrm{LBES}} & P_t^{\mathrm{G,I}} \ge 0 \\ P_{\mathrm{M}}^{\mathrm{LBES}} + P_t^{\mathrm{G,I}} & -2P_{\mathrm{M}}^{\mathrm{LBES}} < P_t^{\mathrm{G,I}} < 0 \\ -P_{\mathrm{M}}^{\mathrm{LBES}} & P_t^{\mathrm{G,I}} \le -2P_{\mathrm{M}}^{\mathrm{LBES}} \end{cases} \tag{29}$$

where $P_{\mathrm{MD},t}^{\mathrm{LBES}}$ is the maximum discharging power of LBES during period t with a time resolution of 1 s.

Then, $P_{\mathrm{MD},t}^{\mathrm{LBES}}$ can be converted into $P_{\mathrm{MD},T}^{\mathrm{LBES}}$ with a time resolution of 15 min through (7). The adjusted maximum discharging power constraint for LBES is introduced into the power supply and demand balance model used for the second model solution.

2) The second load check after the second model solution aims to address the issue of constraint violation beyond the regulation range of the power grid and LBES, which may result in photovoltaic power curtailment.

Through (7), the power of LBES in the second operational results with a time resolution of 15 min can be converted into power with a time resolution of 1 s. But when $P_t^{\mathrm{LBES}} > P_{\mathrm{MD},t}^{\mathrm{LBES}}$, it is necessary to make $P_t^{\mathrm{LBES}} = P_{\mathrm{MD},t}^{\mathrm{LBES}}$ and adjust the power during other periods to ensure that the average power during period T is equal to P_T^{LBES}.

Then, the power output of the power grid in the second load check process with a time resolution of 1 s can be expressed as:

$$P_t^{\mathrm{G,II}} = D_t - P_t^{\mathrm{PV,II}} - P_t^{\mathrm{LBES}} \tag{30}$$

where the superscript II represents the second load check process.

Similar to the first load check, a constraint violation will occur when $P_t^{\mathrm{G,II}} < 0$. And the photovoltaic power curtailment during period t is calculated as:

$$P_t^{\mathrm{PV,curtail}} = -P_t^{\mathrm{G,II}} \quad P_t^{\mathrm{G,II}} < 0 \tag{31}$$

Finally, $P_t^{\mathrm{PV,curtail}}$ can be converted into $P_T^{\mathrm{PV,curtail}}$ with a time resolution of 15 min through (7).

V. Case Study

The test system of the rail transit green energy system is shown in Fig. 1. The measured traction load of a traction substation is shown in Fig. 2. The expected power outputs of the photovoltaic units and non-traction load in the traction substation are shown in Fig. 5.

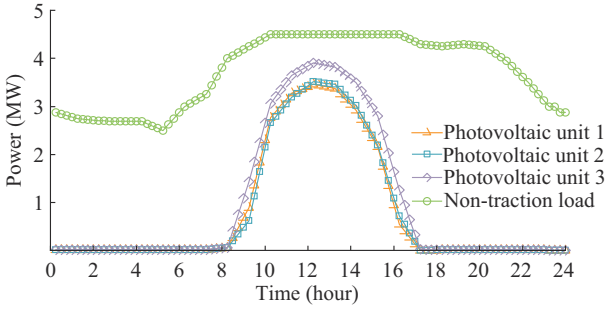

Fig. 5. Expected power outputs of photovoltaic units and non-traction load in traction substation.

TOU electricity price and two-part electricity price are shown in Fig. 6.

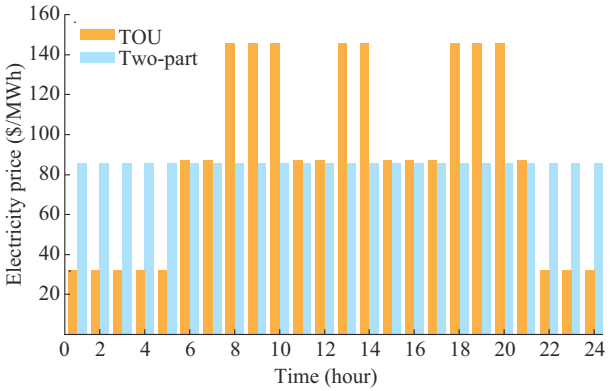

Fig. 6. TOU electricity price and two-part electricity price.

Under the braking condition, the rated power and capacity of SCES are 3 MW and 1 MWh, respectively. Under the traction condition, the rated power and capacity of LBES are 3 MW and 2 MWh, respectively. $W_{\mathrm{C}}^{\mathrm{SCES}}$, $W_{\mathrm{C}}^{\mathrm{LBES}}$, $W_{\mathrm{D}}^{\mathrm{LBES}}$, and $W_{\mathrm{V}}^{\mathrm{PV}}$ are 6.85 \$/MWh, 6.85 \$/MWh, 10.96 \$/MWh, and 6.85 \$/MWh, respectively [28] - [30]. The risk scaling factors of the photovoltaic power output in the low-risk area and the high-risk area are 0.8 and 1.2, respectively. The model is coded with the YALMIP toolbox in MATLAB environment and solved by commercial optimization software GUROBI.

A. Analysis of Regenerative Braking Energy Utilization Model

In this subsection, three different sets of the rated power and capacity for SCES (denoted as sets 1-3) are used, i.e., (1 MW, 1 MWh), (3 MW, 1 MWh), and (3 MW, 2 MWh). The utilization efficiency, economic profit, and carbon dioxide emission reduction of the regenerative braking energy utilization model with such sets are shown in Fig. 7, where the total regenerative braking energy in the traction load is 6.17 MWh, and the carbon dioxide emission reduction per MWh of electricity utilized is 0.858 t.

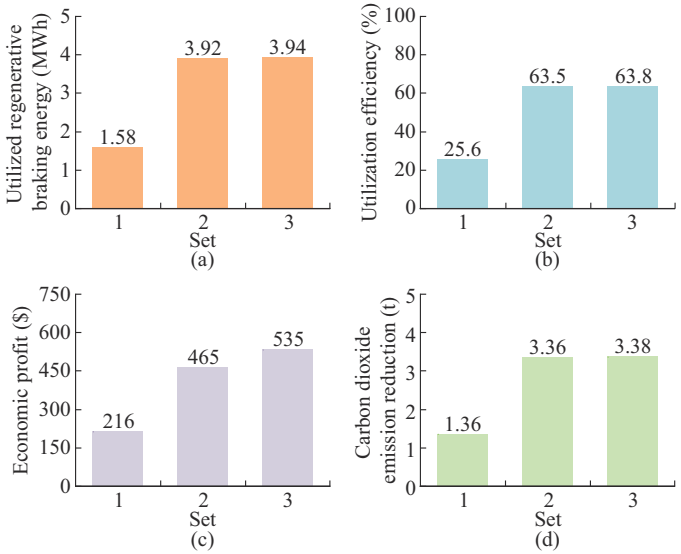

Fig. 7. Analysis of regenerative braking energy utilization model with different sets of rated power and capacity for SCES. (a) Utilized regenerative braking energy. (b) Utilization efficiency. (c) Economic profit. (d) Carbon dioxide emission reduction.

From Fig. 7, it can be observed that the higher the rated power and capacity of SCES, the greater the utilization efficiency, economic profit, and carbon dioxide emission reduction of the regenerative braking energy utilization model. Furthermore, there is a similar utilization efficiency but different economic profits in the results of sets 2 and 3, resulting from the impact of TOU electricity price. Figure 8 shows the power of SCES in the solution results of the above two sets, from which we can find that, as the rated capacity of SCES increases, the discharging power of SCES is more concentrated during the peak electricity price period, which improves the economic profit of the regenerative braking energy utilization model while compensating for non-traction load.

B. Analysis of Power Supply and Demand Balance Model Based on ILR Optimization

1) Cost Comparison with Different ILR Model Parameters

Considering that risk mainly comes from the uncertainty of photovoltaic power output, two different sets of the total fluctuation amount from 07:00 to 17:00 (denoted as sets 4 and 5) are used, as shown in Fig. 9, where 1-3 denote the total amount of fluctuations. And it is easy to find that the value of set 4 is smaller than that of set 5, which means the smaller the fluctuation range, the smaller the risk area and the higher the predictive accuracy of the photovoltaic power output.

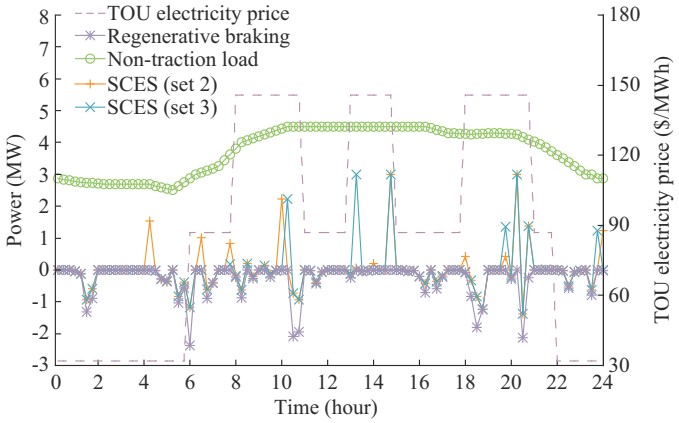

Fig. 8. Solution results of regenerative braking energy utilization model.

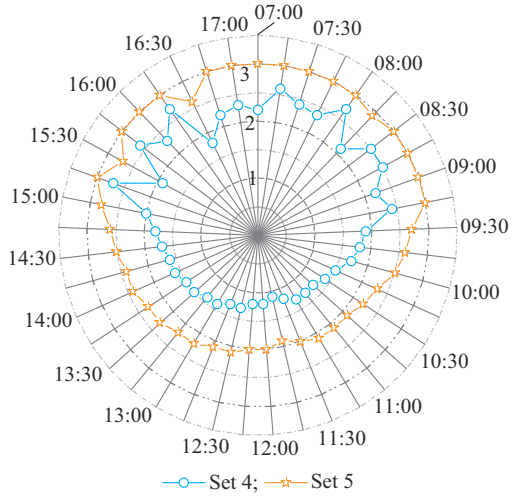

Fig. 9. Total amount of photovoltaic power output fluctuations.

Additionally, we compare the cost of sets 4 and 5, as shown in Table I, from which we can find that the risk cost of set 4 is significantly lower than that of set 5, which means that improving the predictive accuracy can reduce the risk of photovoltaic power output fluctuation, resulting in the lower total cost of the rail transit green energy system.

With set 4, three different sets of the risk scaling factors of the photovoltaic power output in the low-risk area and the high-risk area (denoted as sets 6-8) are used, i.e., (0.8, 1.2), (1.05, 1.2), and (1.15, 1.2). And the cost comparison of sets 6-8 is shown in Table II, from which it is easy to find that when the risk scaling factor in the low-risk area increases from 0.8 to 1.05, the risk cost increases by 31.15%, while when the risk scaling factor in the low-risk area increases from 1.05 to 1.15, the risk cost decreases to 0 but the total cost increases by $250.16. Due to the high risk of the photovoltaic power output at this time, it is believed that the cost of absorbing distributed photovoltaic power is greater than that of directly purchasing electricity from the power grid. Besides, the curtailment of the photovoltaic power and the increased cost of purchasing electricity from the power grid have to be considered, resulting in increased operation costs. The impact of the risk scaling factor in the high-risk area is similar to the above, and repetitive analysis is not conducted.

TABLE I
COST COMPARISON WITH DIFFERENT SETS OF TOTAL AMOUNT OF FLUCTUATIONS

Set	Operation cost ($)	Risk cost ($)	Total cost ($)
4	35466.56	142.48	35609.04
5	35474.78	220.84	35695.62

TABLE II
COST COMPARISON WITH DIFFERENT SETS OF RISK SCALING FACTORS

Set	Operation cost ($)	Risk cost ($)	Total cost ($)
6	35466.56	142.48	35609.04
7	35469.30	186.87	35656.17
8	35906.33	0	35906.33

2) Analysis of Operational Results with Load Check on Second-level Time Scale

To evaluate the reliability of the operational results with load check on the second-level time scale, we select a typical period from 12:30 to 12:45 for analysis, during which the average comprehensive load is 27.17 MW, as shown in Fig. 10(a).

When the comprehensive load with a time resolution of 1 s is above or slightly below its average value of 15 min, the power balance constraint of the system can be met by solely increasing or decreasing the output of the power grid. In the situation, the LBES is discharging at its rated power and the photovoltaic power is fully absorbed, as shown in Fig. 10(b) and (c).

When the comprehensive load with a time resolution of 1 s is far lower than its average value of 15 min, it is insufficient to maintain the system power balance by only decreasing the output of the power grid. As the output of the power grid drops to 0, the LBES rapidly transitions from discharging to charging status, and the photovoltaic power curtailment is conducted if it exceeds the regulation range of the power grid and LBES, as shown in Fig. 10(d) and (e).

Furthermore, the operational results of the first model solution and the second load check during the typical period mentioned above are compared, as shown in Table III. The photovoltaic power decreases slightly after the second load check, due to the abrupt drops in comprehensive load. And the total curtailed photovoltaic power is 32.5 kWh during the typical period.

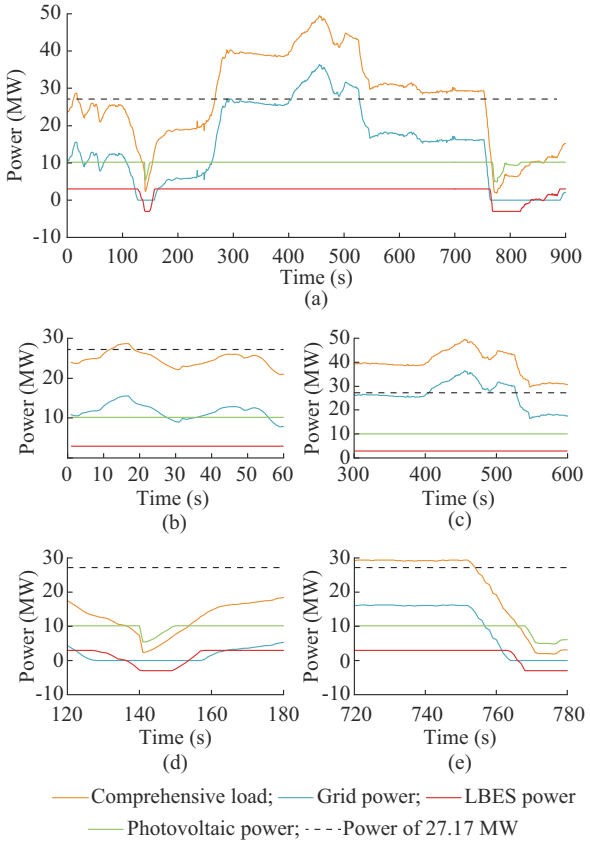

Fig. 10. Operational results during a typical period. (a) 12:30-12:45. (b) 12:30-12:31. (c) 12:35-12:40. (d) 12:32-12:33. (e) 12:42-12:43.

TABLE III
COMPARISON OF OPERATIONAL RESULTS DURING TYPICAL PERIOD

Operation	Comprehensive load (MW)	Grid power (MW)	LBES power (MW)	Photovoltaic power (MW)
First solution	27.17	14.03	3.00	10.14
Second check	27.17	14.84	2.32	10.01

VI. CONCLUSION

The renewable energy resources along the railway can be effectively utilized by integrating photovoltaic power into the TPSS, thus building the rail transit green energy system. However, the uncertainty of photovoltaic power output may pose a risk to the TPSS. To this end, we propose an operation strategy for the rail transit green energy system considering the uncertainty risk of photovoltaic power output. By analyzing the measured data of a specific traction substation as the test system, the following conclusions are drawn.

1) To enhance the utilization efficiency and economic profit of regenerative braking energy, the operation strategy of SCES under the braking condition is optimized by considering the impact of TOU electricity price.

2) The issue arising from different time resolutions between photovoltaic power and traction load is resolved through the implementation of a two-step load check on the second-level time scale. This coordinated optimization addresses the risk associated with photovoltaic operation and the fluctuations in traction load, thereby achieving a balance between risk cost and operation cost.

3) The ILR model can be solved by commercial optimization software in only 4.38 s after linearization, demonstrating a good model-solving performance of the proposed operation strategy.

Focusing on the impact of photovoltaic power output uncertainty on the rail transit green energy system, the control methods and topology structure of the system are not discussed. How to implement the proposed operation strategy through control methods will be the future research direction.

REFERENCES

[1] L. Jia, P. Cheng, Z. Zhang *et al.*, "Integrated development of rail transit and energies in China: development paths and strategies," *Strategic Study of CAE*, vol. 24, no. 3, p. 173, Jul. 2022.
[2] X. Xiao, J. Yin, L. Chen *et al.*, "Evolutionary game-theoretic modeling of massive distributed renewable energy deployment towards low-carbon distribution networks," *Journal of Modern Power Systems and Clean Energy*, vol. 11, no. 5, pp. 1519-1528, Sept. 2023.
[3] Y. Zhang, Y. Han, D. Liu *et al.*, "Low-carbon economic dispatch of electricity-heat-gas integrated energy systems based on deep reinforcement learning," *Journal of Modern Power Systems and Clean Energy*, vol. 11, no. 6, pp. 1827-1841, Nov. 2023.
[4] X. Guo, S. Lou, Y. Wu *et al.*, "Low-carbon operation of combined heat and power integrated plants based on solar-assisted carbon capture," *Journal of Modern Power Systems and Clean Energy*, vol. 10, no. 5, pp. 1138-1151, Sept. 2022.
[5] M. Wu, "Research on photovoltaic generation technology and its economic performance in electrified railway," M.S. dissertation, School of Electrical Engineering, Southwest Jiaotong University, Chengdu, China, 2018.
[6] W. Chen, X. Wang, Q. Li *et al.*, "Review on the development status of PV power station accessing to traction power supply system for rail transit," *Power System Technology*, vol. 43, no. 10, pp. 3663-3670, Oct. 2019.
[7] W. Deng, C. Dai, and W. Chen, "Application of PV generation in AC/DC traction power supply system and the key problem analysis under the background of rail transit energy internet," *Proceedings of the CSEE*, vol. 39, no. 19, pp. 5692-5702, Oct. 2019.
[8] Z. He, D. Feng, S. Lin *et al.*, "Research on security risk assessment for traction power supply system of high-speed railway," *Journal of Southwest Jiaotong University*, vol. 51, no. 3, pp. 418-429, Jun. 2016.
[9] J. A. Aguado, A. J. S. Racero, and S. de la Torre, "Optimal operation of electric railways with renewable energy and electric storage systems," *IEEE Transactions on Smart Grid*, vol. 9, no. 2, pp. 993-1001, Mar. 2018.
[10] M. Wu, Y. Gao, W. Deng *et al.*, "Study of PV generation application on AC powered traction system," in *Proceedings of 2017 Chinese Automation Congress*, Jinan, China, Oct. 2017, pp. 1641-1646.
[11] W. Deng, C. Dai, H. Zhang *et al.*, "Research on comprehensive optimization control method for traction photovoltaic generation system of complex electrified railway," *Proceedings of the CSEE*, vol. 40, no. 18, pp. 5849-5865, Sept. 2020.
[12] W. Deng, C. Dai, and W. Chen, "Preliminary research of multiple constriction for PV access traction power supply system," *Acta Energiae Solaris Sinica*, vol. 41, no. 8, pp. 192-203, Aug. 2020.
[13] H. Hu, J. Chen, Y. Ge *et al.*, "Research on regenerative braking energy storage and utilization technology for high-speed railways," *Proceedings of the CSEE*, vol. 40, no. 1, pp. 246-256, Jan. 2020.
[14] X. Shen and H. Wei, "Study of regenerative braking energy flowing of urban rail transit based on bypass DC loop," *Transactions of China Electrotechnical Society*, vol. 36, no. 15, pp. 3308-3316, Aug. 2021.
[15] J. Zou, S. Ahmed, and X. Sun, "Multistage stochastic unit commitment using stochastic dual dynamic integer programming," *IEEE Transactions on Power Systems*, vol. 34, no. 3, pp. 1814-1823, May 2019.
[16] B. Wang, Z. Qiu, X. Cong *et al.*, "Mechanism analysis of flexible resources' marginal price in new energy grid based on two-stage stochastic optimization modeling," *Proceedings of the CSEE*, vol. 41, no. 4, pp. 1348-1359, Feb. 2021.
[17] Z. Zhang, Y. Chen, F. Liu *et al.*, "Two-stage robust unit commitment model considering operation risk and demand response," *Proceedings*

of the CSEE, vol. 41, no. 3, pp. 961-973, Feb. 2021.
[18] M. Fischetti and M. Monaci, "Light robustness," in *Robust and Online Large-scale Optimization*. Berlin: Springer, 2009, pp. 61-84.
[19] L. Qin, J. Lin, S. Dai *et al*., "An improved light robust optimization model and its linear counterpart," *Proceedings of the CSEE*, vol. 36, no. 13, pp. 3463-3469, Jul. 2016.
[20] Y. Zhang, X. Lin, Z. Xu *et al*., "Dispatching method of micro-energy grid based on light robust optimization," *Automation of Electric Power Systems*, vol. 42, no. 14, pp. 75-82, Jul. 2018.
[21] L. Qin, J. Lin, S. Dai *et al*., "Improved light robust optimization model based wind-thermal unit commitment," *Proceedings of the CSEE*, vol. 36, no. 15, pp. 4108-4119, Aug. 2016.
[22] D. Feng, S. Lin, X. Sun *et al*., "Reliability assessment for traction transformer considering load characteristics of high-speed railway," *Journal of the China Railway Society*, vol. 39, no. 8, pp. 62-69, Aug. 2017.
[23] B. Wei, H. Hu, K. Wang *et al*., "Research on traction load forecasting method for high-speed railway traction substation based on measured data and train timetable," *Transactions of China Electrotechnical Society*, vol. 35, no. 1, pp. 179-188, Jan. 2020.
[24] L. Zhang, Q. Li, and Y. Zhu, "Prediction of traction load for new electrified railway," *Journal of Southwest Jiaotong University*, vol. 51, no. 4, pp. 743-749, Aug. 2016.
[25] S. Zhao, T. Zhang, Z. Li *et al*., "Distribution model of day-ahead photovoltaic power forecasting error based on numerical characteristic clustering," *Automation of Electric Power Systems*, vol. 43, no. 13, pp. 36-45, Jul. 2019.
[26] Y. Liu, Y. Chen, H. Tian *et al*., "New energy and energy storage planning and configuration in rail transportation self-sufficient energy systems based on two-stage robust optimization," *High Voltage Engineering*, doi: doi.org/10.13336/j.1003-6520.hve.20231304
[27] *Technical Requirements for Connecting Photovoltaic Power Station to Power System*, GB/T 19964-2024, 2024.
[28] Y. Chen, Y. Yao, and Y. Zhang, "A robust state estimation method based on SOCP for integrated electricity-heat system," *IEEE Transactions on Smart Grid*, vol. 12, no. 1, pp. 810-820, Jan. 2021.
[29] Y. Chen, J. Ma, P. Zhang *et al*., "Robust state estimator based on maximum exponential absolute value," *IEEE Transactions on Smart Grid*, vol. 8, no. 4, pp. 1537-1544, Jul. 2017.
[30] H. Zhang, D. Yue, C. Dou *et al*., "Resilient optimal defensive strategy of TSK fuzzy-model-based microgrids' system via a novel reinforcement learning approach," *IEEE Transactions on Neural Networks and Learning Systems*, vol. 34, no. 4, pp. 1921-1931, Apr. 2023.

Yanbo Chen received the B.S. degree in electrical engineering from Huazhong University of Science and Technology, Wuhan, China, in 2007, the M.S. degree in electrical engineering from China Electric Power Research Institute, Beijing, China, in 2010, and the Ph.D. degree in electrical engineering from Tsinghua University, Beijing, China, in 2013. He is currently a Professor with School of Electrical and Electronic Engineering, North China Electric Power University, Beijing, China. His research interests include power system state estimation and optimal power flow.

Haoxin Tian received the B.S. and M.S. degrees in electrical engineering from North China Electric Power University, Baoding, China, in 2018 and 2021, respectively. He is currently pursuing the Ph.D. degree in electrical engineering at North China Electric Power University, Beijing, China. His research interests include planning and operation of power systems with renewable energy.

Guodong Zheng received the B.S. degree from North China Electric Power University, Baoding, China, in 2020, and the M.S. degree in electrical engineering from North China Electric Power University, Beijing, China, in 2023. He is currently an Electrical Engineer with State Grid Changsha Power Supply Company, Changsha, China. His research interests include operation strategy and risk assessment of rail transit green energy system.

Yuxiang Liu received the B.S. degree from North China Electric Power University, Beijing, China, in 2021. He is currently pursuing the M.S. degree in electrical engineering at North China Electric Power University. His research interests include planning and configuration of new energy and energy storage of rail transit green energy system.

Maja Grbić received the B.S., M.S., and Ph.D. degrees in electrical engineering from School of Electrical Engineering, University of Belgrade, Belgrade, Serbia, in 2010, 2012, and 2021, respectively. She is currently a Research Associate with Nikola Tesla Electrical Engineering Institute, University of Belgrade. Her research interests include power system analysis and control.